Chem Rev Lett 6 (2023) 147-162

Research Article

Chemical Review and Letters
journal homepage: www.chemrevlett.com
ISSN (online): 2645-4947 (print) 2676-7279

Split Plot Central Composite Design for Optimization of 4-Bromophenol Adsorption from Synthetic Wastewater, using Synthesized $BiFeO_3$ Perovskite Material

Zaharaddeen Nasiru Garba[1,] *, Godwill Stephen[1] and Patricia Adamma Ekwumemgbo[1]

[1]*Department of Chemistry, Ahmadu Bello University, P.M.B. 1044, Zaria, Nigeria*

ARTICLE INFO

Article history:
Received 23 January 2023
Received in revised form 16 April 2023
Accepted 20 April 2022
Available online 10 August 2023

Keywords:
Split-plot central composite design
Bismuth ferrite perovskite
Adsorption
Optimization
4-Bromophenol

ABSTRACT

Optimizing adsorption processes with the use of standard central composite designs (CCD) for the removal of contaminants from wastewater is becoming more popular. The use of standard CCD enables the variables under study to be randomized. However, some studies, particularly those conducted within industries, usually involve factors with some hard to change (HTC) levels and others with easy to change (ETC) levels, in which case the HTC factor cannot be totally randomized, resulting in a split-plot design. The optimum conditions for the removal of 4-bromophenol (4-BP) from synthetic wastewater onto $BiFeO_3$ were investigated in this study using split plot CCD and three adsorption factors (pH, adsorbent dosage, and shaking time) were considered. The pH was considered the HTC factor because of the duration of time, acid and/or base required to change it, whereas the adsorbent dosage and contact time were the ETC variables. Adsorbent dosage of 0.60 g, pH of 7, and contact time of 167 minutes were found to be the optimum adsorption conditions at desirability of 1. The predicted and experimental adsorbed values were 88.02 % and 87.86 %, respectively, indicating that the experimental and predicted values were in good agreement. The equilibrium adsorption data was found to be best suited by the Langmuir isotherm model, yielding a monolayer adsorption capacity of 65.96 mg/g. Regression results, as well as q_e experimental and q_e calculated values, reveal that the pseudo-second-order model more closely represents the kinetics.

1. Introduction

Rapid urbanization, industrialization, and population growth, according to [1] have resulted in organic pollutants infiltrating most water supplies, posing a threat to the environment, human health, and ecological system. The chemical, pharmaceutical, and petroleum processing industries produce the majority of these organic pollutants, with phenol and phenolic wastes being the most common [1] According to [2] Scientists try to find new ways in order to neutralize or remove these chemical agents which damage our environment [3] reported that phenol is an aromatic, weak acidic organic molecule with the chemical formula C_6H_5OH. It's a 33flammable white crystalline compound that occurs in about 2000 different types and can be found in sewage, natural water, and drinking water. The presence of halogen substituted groups in phenol (chloro and bromo)

increases its toxicity, posing a serious health risk and causing major environmental damage [4]. When phenol is electrophilically halogenated with bromine, bromophenol is produced. It is any phenol organobromide with one or more covalently bonded bromine atom. Because of dynamic biogeochemical cycling, organobromines are the most common kinds of bromine on the planet [6]. Toxic pollutants include bromophenol and bromophenol-containing compounds, according to [6,7] and bromophenols were added to the United States Environmental Protection Agency's (USEPA) list of hazardous wastes in 1998. According to [8] phenolic contaminants are very harmful

* Corresponding author.; Tel. +9647504682450; e-mail: nwichun1@gmail.com (Stephen godwill)
https://doi.org/10.22034/crl.2022.326007.1150

even at low concentrations and are one of the most hazardous organic pollutants. Phenols can cause coma, convulsions, cyanosis, and damage to the liver, kidney, lung, and vascular system, among other things, when inhaled, ingested, or absorbed through the skin. Phenolic chemicals, according to [9], are generally harmful and mutagenic at high concentrations. Phenolic compounds are also reported by [10] to be among the substances that cause cancer, respiratory diseases, fibrosis, and pneumonia. As a result, the US Environmental Protection Agency (USEPA) has set a limit of less than 1 mg/L for phenol discharge in order to reduce the risk of phenol [11]. In drinking water, the maximum limit is 0.002 mg/L [12]. As a result, before discharging wastewater into the environment, phenols must be removed.

Several methods for treating wastewater containing phenols and other organic contaminants have been used over the years. Bioremediation has been shown to be a viable and ecologically sustainable method of treating organic contaminants in soil and water [13]. According to [11] oxidation, precipitation, ion exchange, photocatalytic degradation, solvent extraction, and adsorption are some methods utilized to remediate wastewater over time. Activated carbon is the most often utilized adsorbent in the adsorption process [14]. The surface properties of this material are said to be good, with a wide surface area and pore volume. According to reports, activated carbon may contain functional groups that interact with contaminating compounds. It is a useful material for adsorption activities because of these features, as it has a high adsorption capacity [15]. But there is still need to find an adsorbent whose precursors are readily available and easy to prepare. Perovskites nanoparticles have lately been used as adsorbents and researchers have recently become interested in them due to their outstanding properties and potential applications in a variety of fields, including photocatalysis, sensors, CO_2 conversion, dry reforming catalysts, syngas generation, and most recently, adsorption [16]. Response surface methodology, or RSM, has continued to play a vital role in developing, optimizing, and improving processes, particularly with multiple input variables [17]. RSM is a group of mathematical and statistical techniques used in the development of an adequate functional relationship between a response of interest, Y, and a number of associated control (or input) variables denoted by X_1, X_2, X_3… Classic response surface designs, on the other hand, have the drawback of assuming that all elements are equally easy to manipulate, allowing for total randomization of experimental run order. However, due to the presence of some variables with hard-to-change (HTC) levels, most industrial experiments cannot be entirely randomized [18]. As a result, these studies are frequently carried out in a way that limits their randomization, resulting in a split-plot structure. In a split-plot design, experimental runs are performed in groups, where in a group, the levels of the HTC factors are not reset from run to run. This creates dependence among the runs in one group, and leads to clusters of correlated errors and responses. Myers and Lentner published the first publication that focused exclusively on conducting response surface studies with a split-plot structure, as reported by [18]. The efficiency of various second-order response surface designs when executed using a split-plot structure was investigated by the authors. According to [18] other authors such as Vining and Kowalski in 2005 and in 2006 respectively modified completely randomized central composite and Box-Behnken designs to accommodate a split-plot structure. Factorial (f), whole-plot axial (α), subplot axial (β), and center (c) points make up the split-plot central CCD. When compared to the Completely Randomized Design, the split-plot design would provide more precise results at a lower cost [19]. In this study, we used the solution combustion method to synthesize the perovskite $BiFeO_3$ and used split plot central composite design to investigate its optimum 4-bromophenol adsorptive potential (in the absence of light to avoid photooxidation) in the hope of finding a better, easy to prepare, less expensive, and environmentally acceptable material for organic pollution remediation. To our knowledge, there was no literature describing the removal of 4-bromophenol (4-BP) from wastewater using split plot CCD and the sated perovskite.

2.Results and Discussion

The XRD pattern was recorded in the 2θ ranges 5 - 80°C. The X-ray pattern of the synthesized bismuth ferrite powder is shown in Fig 1. The peaks in the XRD patterns were identified as a rhombohedra perovskite structure of $BiFeO_3$ with space group R-3m and Lattice parameters a = b = c = 3.9520 (Å), which corresponds to ICDD reference number 01-072-2112. This is identical with what [20] produced. However, the commonly observed byproducts like $Bi_2Fe_4O_9$, and $Bi_{24}Fe_2O_{39}$ located at 2θ =27.97° [21] were not detected. As a result, the XRD analysis showed that the synthesized $BiFeO_3$ was highly crystalline and pure. The Scherer equation was used to calculate the average crystallite size (D) of $BiFeO_3$ powder (Equation. 1). The average crystallite size as determined by the XRD pattern was 140.20 nm. However, because the width of diffraction peaks is inversely proportional to crystal size, the $BiFeO_3$ peaks identified were fairly sharp, indicating a high degree of crystallinity in the powder and hence the large crystal size [22]. According to literature, the size of $BiFeO_3$ particles can change considerably with heat treatment/temperature [21].

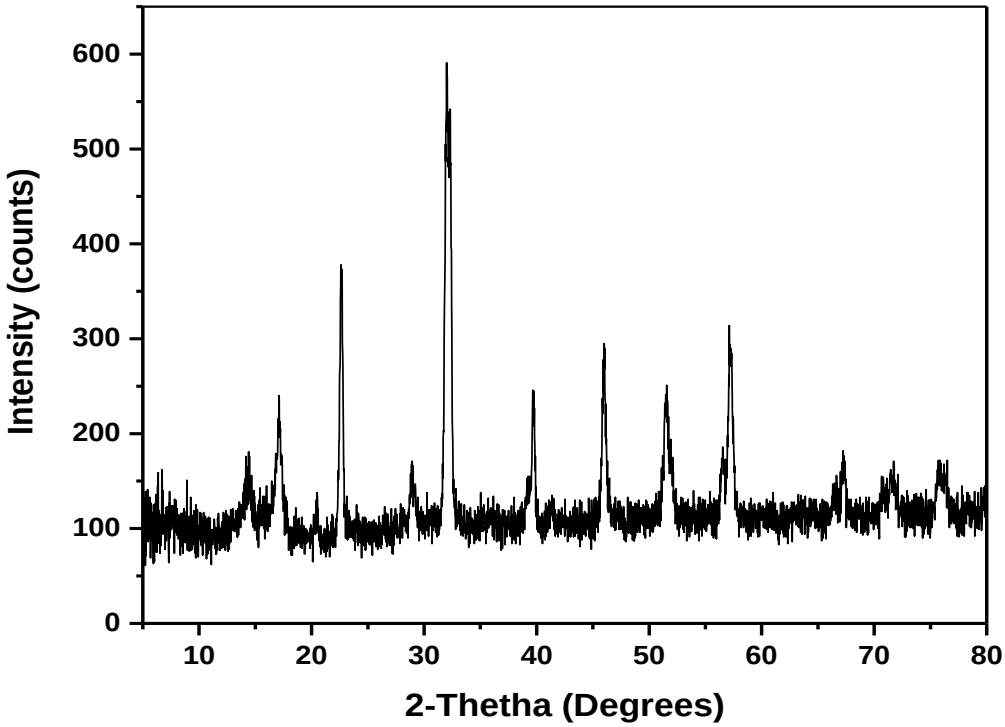

Fig 1. Powder XRD pattern of the prepared $BiFeO_3$ adsorbent.

A scanning electron microscope was used to examine the morphology of the synthesized $BiFeO_3$ at various magnifications (100 and 20 μm) as shown in Fig 2a and 2b for a clear view of the morphology. During the combustion process between fuels and nitrates, a significant amount of gases (NO, NO_2, CO, NH_3, and H_2O) were produced, resulting in agglomerated particles of varied sizes and forms [23]. [24, 25, 26] synthesized and reported $BiFeO_3$ images with morphologies that were similar to ours.

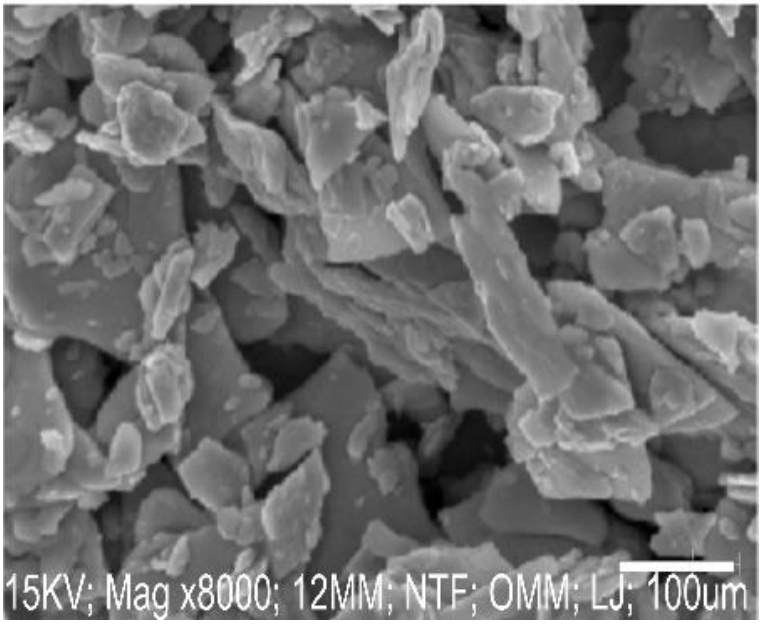

Fig 2a. SEM image of the $BiFeO_3$ at 100 μm magnification

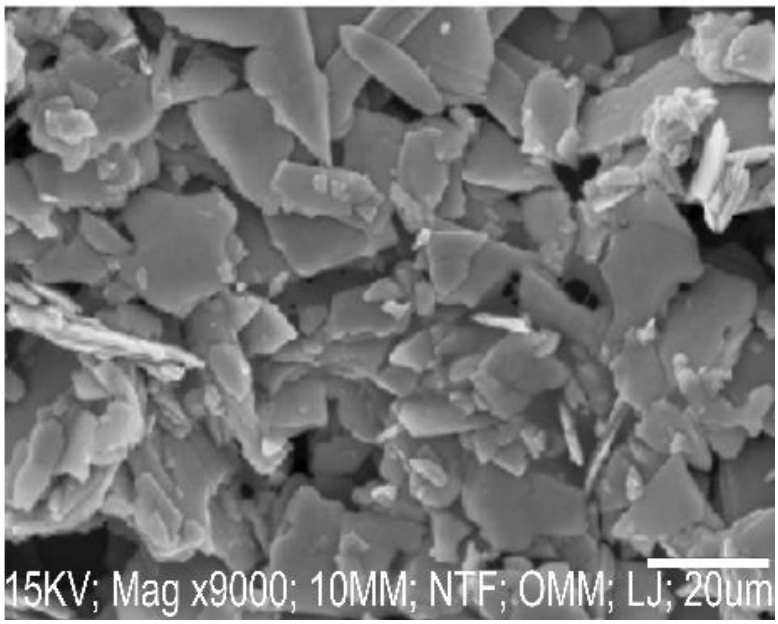

Fig 2b. SEM image of the $BiFeO_3$ at 20 μm magnification

Table 1. Independent Variables and their Levels

Independent variable	**Unit**	**Symbol**	**Levels**				
			-α	**-1**	**0**	**+1**	**+α**
pH		a	2	4	7	10	12
Time	min	B	30	87	165	243	300
Dosage	g	C	0.2	0.4	0.6	0.8	1.0

The design matrix for the HTC and ETC variables, their ranges, and the responses (% removal of 4-BP) are shown in Table 2. Due to the amount of time, acid, and/or base required to adjust the pH, it was chosen as the HTC factor (a) while contact time (B) and adsorbent dosage (C) are the ETC factors. The experimental runs were divided into groups based on the pH (HTC factor). The grouping of HTC factor makes the experiment much easier to run. The whole plot column has been added to keep track of HTC factor combinations, which form the "whole plots". All of the runs in any given group maintain a constant level of the HTC factor. As can be observed from the data, using $BiFeO_3$ as an adsorbent, the percentage removal of 4-BP ranges from 31.36 to 87.86 percent. The regression Equation (Equation 1) for 4-BP was generated using split plot RSM, which describes the functional relationship between 4-BP removal % and process variables.

$$Y_{4-BP} = -161.1 + 31.25a + 0.5998B + 273.4C + 7.22e^{-05}\,aB - 8.9aC + 0.114BC - 1.75a^2 - 0.0019B^2 - 196.18C^2 \quad (1)$$

Where: ($Y_{4\text{-}BP}$) is % of 4-BP adsorbed by $BiFeO_3$, pH (a), Time (B) and adsorbent dosage (C) respectively. ETC factors are represented by capital letters, while HTC factors are represented by small letters. The model's goodness of fit was evaluated using the determination coefficient (R^2), which showed that the model explained nearly 90% of the variation in the observations (R^2= 0.8952) for 4-BP. Fig 3 depicts the relationship between predicted and actual values. The plot shows that the data points were evenly split by the 45 degree line, which helps us detect observations that were not properly predicted by the model.

Table 2. Independent Variables, their Levels and Responses using Split Plot CCD

Run order	Whole plot	a: pH	B:Time (min)	C:Dosage (g)	4-BP Removal
1	1	7	165	0.6	87.86
2		7	165	0.6	87.76
3		7	165	0.6	87.42
4	2	12	165	0.6	50.18
5		12	165	0.6	53.36
6	3	7	165	0.6	87.30
7		7	165	0.6	87.65
8		7	165	0.6	87.41
9	4	4	87	0.8	50.06
10		4	243	0.8	57.16
11		4	243	0.4	49.56
12		4	87	0.4	51.45
13	5	7	165	0.6	87.64
14		7	165	0.6	87.43
15		7	165	0.6	87.58
16	6	10	87	0.4	60.20
17		10	87	0.8	39.13
18		10	243	0.4	62.50
19		10	243	0.8	45.54
20	7	2	165	0.6	31.36
21		2	165	0.6	37.06
22	8	7	165	0.2	59.51
23		7	165	1.0	64.18
24		7	300	0.6	71.58
25		7	30	0.6	42.22

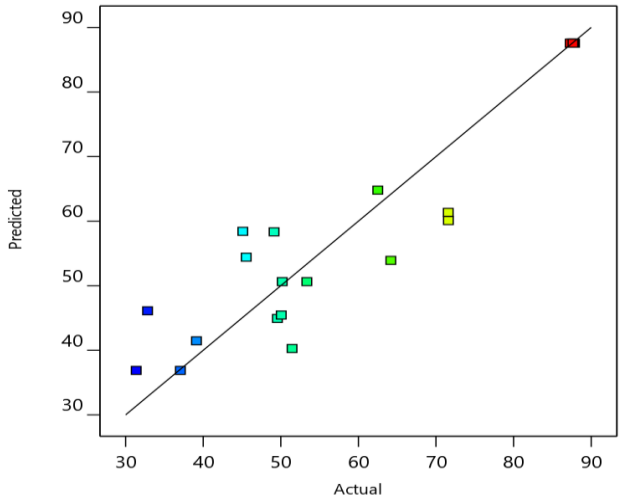

Fig 3. Normal plot showing relationship between the predicted and experimental data for 4-BP adsorption onto $BiFeO_3$

According to [19] special statistical tools such as restricted maximum likelihood (REML) are used to obtain the correct P-values from a split-plot. The goal of maximum likelihood estimation is to find the parameter values that most closely make the observed data. This is another method for calculating variances. REML estimates the group variance for the whole plot factors and the residual variance for the subplot factors in the split-plot case. Once the variances are estimated, Generalized Least Squares (GLS) is used to estimate the factor effects and Kenward-Roger's method is then used to produce F-tests and the corresponding p-values [19]. Table 3 shows the results of the model's restricted maximum likelihood analysis for 4-BP. Variance terms are divided into two sections in this table: a whole-plot section for HTC factors and a subplot section for ETC factors. This result is in line with the findings of [27]. The p-value (Prob > F) for the whole-plots for 4-BP was found to be highly significant, with values much below 0.05, which is the generally accepted alpha value. That is, for all of the terms in the model's whole-plot (HTC) section. Moreover, the subplot terms were found to be highly significant as a whole (with the exception of these few subplot terms; C, aB and BC). The main effects of variables B and C (contact time and adsorbent dosage); the interaction effect of pH and adsorbent dosage (aC); the quadratic effect of B (B^2) and the quadratic effect of C (C^2) were all shown to be highly significant (with p-values far less than 0.05).

Table 3. Restricted Maximum Likelihood (REML) analysis with Kenward-Roger p-values for 4- BP removal by $BiFeO_3$

Source	Term df	Error df	F-value	P-value	Remark
Whole-plot	2	5.67	92.76	< 0.0001	Significant
a-pH	1	5.38	5.73	0.0585	
a^2	1	5.99	179.82	< 0.0001	
Subplot	7	10.17	16.00	< 0.0001	Significant
B-Tim	1	11.02	11.90	0.0054	
C-Dosage	1	11.02	1.60	0.2323	
aB	1	11.02	0.0608	0.8097	
aC	1	11.02	9.72	0.0098	
BC	1	11.02	0.8522	0.3757	
B^2	1	9.00	64.97	< 0.0001	
C^2	1	9.00	46.40	< 0.0001	

For batch adsorption processes, optimum adsorption conditions are important, hence the optimization of 4-BP adsorption onto the synthesized $BiFeO_3$ was done with design-expert software (version 12). The maximum values for the response were used as the target criterion in the optimization analysis [28]. As shown in Table 5, the best adsorption conditions were pH 7, contact time of 167 minutes, adsorbent dose of 0.6 g, and desirability of 1. The

model validation results demonstrate that at the optimum conditions, the experimental (actual) percent adsorbed values for 4-BP obtained in the laboratory was only slightly lower than those predicted, indicating good agreement between experimental and model values. The usage of the model will save time because fewer laboratory experiments will be necessary [25]

Table 4. Values for the Process Optimization

Desirability	Parameters			Predicted value	Actual value
	pH	Time (min)	Dosage (g)		
1	7	167	0.6	88.02	87.86

3D surface response was used to investigate the interactive relationship between independent variables and response. Fig 4a depicts the effect of contact time and adsorbent dosage on 4-BP removal (pH 7). It can be seen that with both contact time and adsorbent dosage playing essential roles, removal of 4-BP above 80% can be obtained. As the time increases, it becomes obvious that increasing the adsorbent dosage from 0.37 to 0.83 g had a considerable impact on 4-BP removal, with optimum removal happening at about 0.65 g. The increase in percent removal can be attributable to the adsorbent's increased surface area and adsorption sites. The amount of 4-BP removed began to slightly decrease as the dosage was increased further. This can be ascribed to adsorbent saturation and possibly agglomeration [29]. Fig 4b shows that both pH and adsorbent dose played a significant role in achieving a percent adsorbed value above 80%. (Holding contact time at 165 min). The improvement in 4-BP removal efficiency can be attributed to an increase in both adsorbent dose and pH at the same time. According to [30], optimum adoption occurs at higher pH because most 4-BP ions are protonated at low pH, and the adsorbent surface is partially positively charged. As a result, electrostatic repulsion occurs, causing the adsorption to be poor. Hence, at higher pH, there is an increased contribution of OH^- free ions, which are attracted to the adsorbent and tend to make it negatively charged, resulting in an electrostatic interaction between the 4-BP and the adsorbent until the adsorbent is saturated. Fig 3c shows the removal of 4-BP as a function of pH and time, with a percent adsorbed value of more than 80% attained at a pH of 7.6 and a contact time of 165 minutes (keeping adsorbent dosage at 0.6 g). It can be seen from the 3D surface response (Fig 4c) that both factors have similar impacts on the adsorbent removal percent, with an increase in pH and time leading to an increase in percent removal.

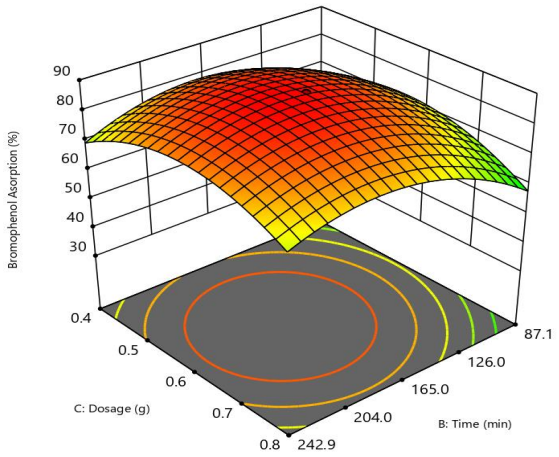

Fig 4a. 3D Response surface for interaction between time and dosage for 4-BP adsorption

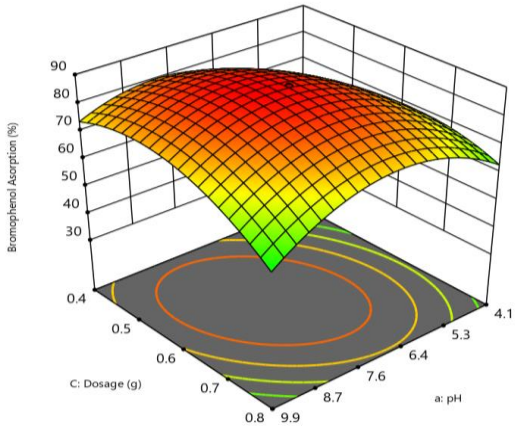

Fig 4b. 3D Response surface for interaction between pH and dosage for 4-BP adsorption

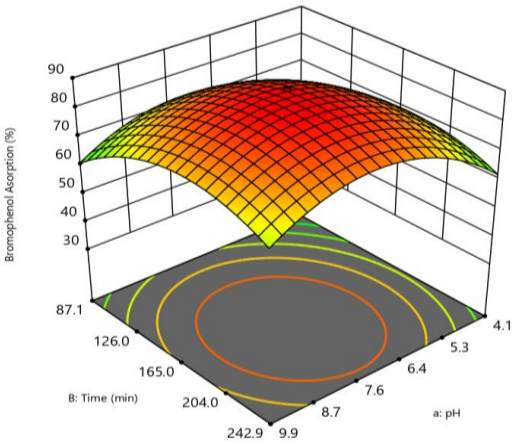

Fig 4c. 3D Response surface for interaction between time and pH for 4-BP adsorption

Data from equilibrium studies carried out at ambient temperature with varied initial concentrations of the adsorbate were used to test the applicability of the Langmuir, Temkin, and Freundlich isotherms under the optimal conditions (Table 5). A plot of $1/q_e$ versus $1/Ce$ of the Langmuir model (Fig 5) gave a straight line with $1/q_{max}$ as intercept and $1/K_L q_{max}$ as slope, and hence q_{max} and K_L were estimated (Table 6). For the Langmuir model, the constants K_L and q_{max} are the adsorption equilibrium constant (mg/L) and monolayer adsorption capacity of the adsorbent (mg/g), respectively. The values of these constants were derived from the slope and intercept of the Langmuir plot and are shown in Table 6. The linear Langmuir plot (Fig 5) yielded a q_{max} value of 106.50 mg/g for phenol. The R_L is a critical element of the Langmuir isotherm since it indicates the isotherm shape and predicts whether an adsorption system is favorable or unfavorable. R_L may be determined using equation 5 according to [29]. Fig 6 shows a Freundlich plot of log q_e vs log C_e for various adsorption data for the adsorbate onto the $BiFeO_3$ adsorbent. Table 6 shows the numerical values for the plot's constants n and K_f, which were calculated using the plot's slope and intercept. The constant K_f is also known as the adsorption or distribution coefficient, and it represents the adsorbent's relative adsorption capacity in relation to the bonding energy. For a given unit equilibrium concentration, it denotes the amount of adsorbate that has been adsorbed onto the adsorbent.

For the Temkin model, plotting q_e versus lnC_e, Equation (7) resulted in a straight line of slope $^{RT}/_{b_T}$ and intercept $^{RT}/_{b_T} lnK_T$

Fig 7 shows the Temkin isotherm plot, with the evaluated isotherm parameters listed in Table 6. The wide range in R^2 observed among the different isotherms tested plainly demonstrated that the Temkin equation does not fit the equilibrium experimental data satisfactorily. According to the fitting findings shown in Table 6, the Langmuir isotherm model appeared to be much more applicable than the Freundlich and Temkin models with the greatest R^2 value. The Langmuir model's applicability to the adsorption process implies that the adsorbate's ion molecules from bulk solution were adsorbed on a homogenous monolayer.

As can also be seen from Table 6 the R_L value lies between 0 and 1 which confirms the adsorption processes to be favourable (physisorption) under the studied conditions. Table 7 shows the comparison of the maximum monolayer adsorption of phenols onto various adsorbents.

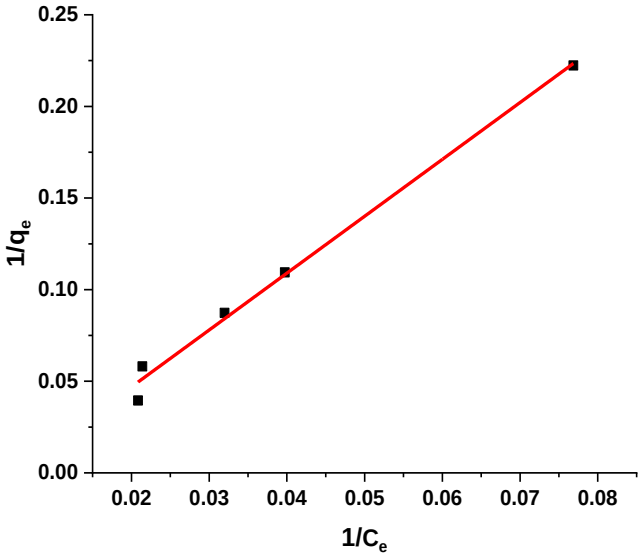

Fig 5. Langmuir isotherm plot for 4-BP adsorption onto $BiFeO_3$

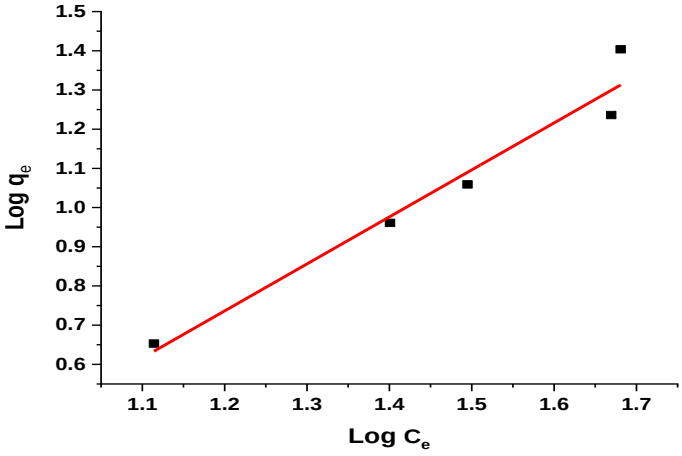

Fig 6. Freundlich isotherm plot for 4-BP adsorption onto $BiFeO_3$

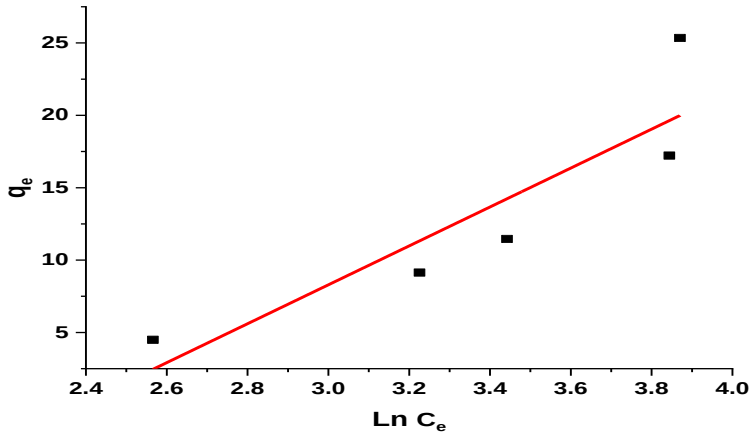

Fig 7. Temkin isotherm plot for 4-BP adsorption on $BiFeO_3$

Table 5. Langmuir, Freundlich and Temkin Isotherm Model Parameters for 4-BP Adsorption

Isotherm	Parameters	Values
Langmuir	q_{max} (mg/g)	65.96
	K_L (L/mg)	0.0049
	R_L	0.8366
	R^2	0.9896
Freundlich	K_f (L/mg)	0.1986
	n	0.8341
	R^2	0.9430
Temkin	B_T (J/mol)	13.4412
	K_T (L/mg)	0.0923
	R^2	0.7358

Table 6. Comparison of the maximum monolayer adsorption of phenols onto various adsorbents

Adsorbent	adsorbate	q_{max} (mg/g)	Reference
Granular activated carbon	Phenol	214.13	[31]
Acacia leucocephala bark powder	2-Chlorophenol	147.05	[32]
Poly(ether-block-amide) copolymer	4-Bromophenol	2.57	[33]
Olive mill waste	Phenol	62.5	[34]
Treated tea waste	Phenol	2.801	[35]
Poly(ether-block-amide) copolymer	2,6-Dibromophenol	4.55	[33]
sewage sludge based adsorbent	Phenol	26.16	[36]
Poly(ether-block-amide) copolymer	2,4,6-Tribromophenol	5.26	[33]
$BiFeO_3$	4-Bromophenol	69.96	This work
$BiFeO_3$	Phenol	106.50	[37]

Adsorption kinetics is the study of how much a substance absorbs over time at a constant concentration. Pseudo-first-order and pseudo-second-order models were used to Fig out how the adsorption process works. The pseudo-first-order model, which posits that the rate of adsorption site occupation is proportional to the number of unoccupied sites, is expressed using the Lagergren equation [38]. A plot of $\ln(q_e - q_t)$ versus t (Fig 8) was used to estimate the values of k_1 and q_e from the slope and the intercept, respectively (Table 8). On the other hand, the

pseudo-second-order kinetic model was expressed in the linear form by Equation 9. Where K_2 is the equilibrium rate constant of pseudo-second-order model (g/mg min^{-1}). The values of q_e and K_2 (Table 8) were determined from the slope and intercept of the plot of (t/q_t) versus t respectively (Fig 9). The correlation coefficient (R^2) was 0.968 and R^2 0.988 for the pseudo-first-order and pseudo-second-order kinetic models respectively, suggesting the applicability of the pseudo-second-order kinetic model to the adsorption of phenol. The q_e calculated value for 4-BP (6.90 mg/g) for the pseudo-second-order kinetic reaction was found to be in better agreement with the q_e experimental. values (5.91 mg/g) further confirming the fitting of the data to the pseudo-second order model. K_2 value of 4-BP was 0.021, indicating faster adsorption rate of the adsorbate by the $BiFeO_3$.

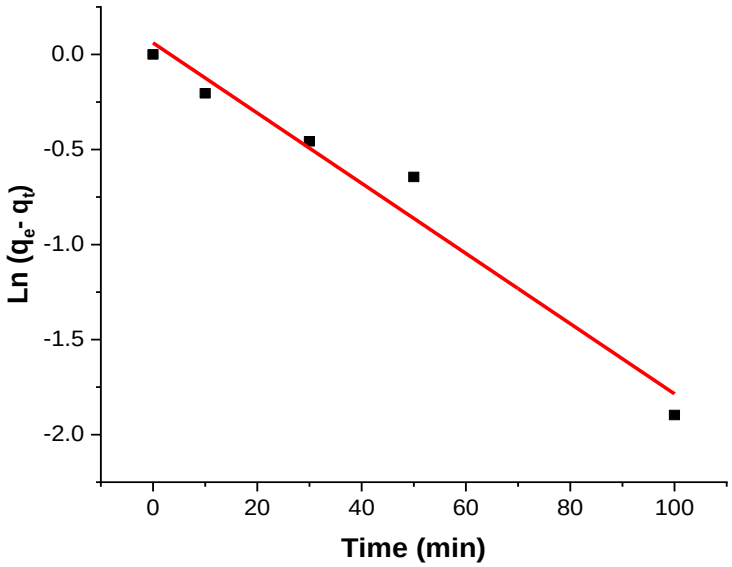

Fig 8. Pseudo-first-order kinetic model for 4-BP

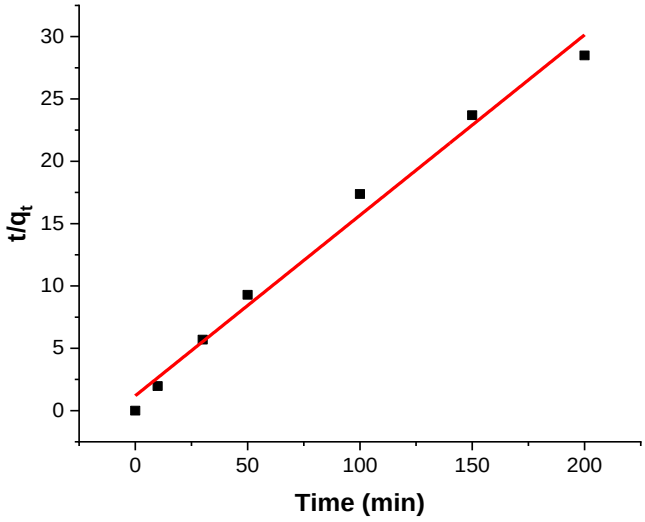

Fig 9. Pseudo-second-order kinetic model for 4-BP

Table 7. Calculated values of the various kinetic models' constants and their correlation coefficients (R^2) for the adsorption of 4-BP onto $BiFeO_3$

Kinetic model	Parameter	Value
Pseudo-first-order	$q_{e\ cal.}$	1.06
	$q_{e\ exp.}$	5.91
	K_1	0.000092
	R^2	0.968
Pseudo-second-order	$q_{e\ cal.}$	6.90
	$q_{e\ exp.}$	5.91
	K_2	0.021
	R^2	0.988

3.Experimental

3.1. Materials

All the reagents used in this study were of analytical grade and used without further purification. The reagents include: Bismuth nitrate pentahydrate, $Bi(NO_3)_3.5H_2O$; Iron nitrate nanohydrate, $Fe(NO_3)_3.9H_2O$; Nitric acid, HNO_3; Glycine, $C_2H_5NO_2$; Urea, CH_4N_2O; Sodium hydroxide, NaOH; Hydrogen chloride, HCl and 4-Bromophenol, C_6H_5BrO. While The equipment used include: X-ray diffractometer (XRD), Scanning Electron Microscopy (SEM), Double beam UV/Vis spectrophotometer, Muffle furnace, Mechanical Shaker, Heating mantle, pH meter, Magnetic stirrer, Analytical weighing balance, Porcelain dish, filter paper and other commonly used laboratory apparatuses

3.2. Preparation of $BiFeO_3$ Perovskite Material

[24] described a solution combustion method for producing $BiFeO_3$ perovskite nanomaterial The solution combustion approach takes less time, is easier to use, and delivers a high synthesis rate for the target compounds, indicating superior performance in material [39]. [40] stated that the method is easy, energy efficient, cost effective, and requires lower process temperatures than other methods. First, 200 ml solutions of the corresponding precursors were made by weighing and dissolving the requisite amounts (obtained from the equation of the reaction) of the compounds in little amount of distilled water. Few drops of nitric acid were added and the solutions were swirled using magnetic stirrer until a uniform mixture was formed, then more distilled water was added to make it up to the 200 ml mark of the volumetric flask. Then, the prepared solutions of $Bi(NO_3)_3.5H_2O$ and $Fe(NO_3)_3.9H_2O$ were combined at room temperature with magnetic stirring, and addition of the glycine and urea fuels in the correct stoichiometry as specified in the reaction equation. Drops of dilute nitric acid were added next, and the mixture was agitated until it became clear:

$$6Bi(NO_3)_3.5H_2O + 6Fe(NO_3)_3.9H_2O + 10C_2H_5NO_2 + 15CH_4N_2O \rightarrow 6BiFeO_3 + 35CO_2 + 38N_2 + 139H_2O$$

The temperature was progressively raised to 400°C by placing the entire mixture in a porcelain dish and placing it on a heating mantle. The mixture was heated until the solvent had evaporated completely, and a combustion reaction occurred, releasing a large amount of gas and forming a brownish powder. After that, the brownish powder was placed in a muffle furnace and thermally treated for 1 hour at 500°C with a 2°C/min ramp. The powder formed from heat treatment was allowed to cool before being removed for characterization and application.

3.3. Characterization of the $BiFeO_3$ Perovskite

The crystal structure of the $BiFeO_3$ perovskite was characterized using a powder diffractometer equipped with Cu Kα (λ=1.5406 Å) as the radiation source. The XRD pattern was observed in the 2θ ranges 5 - 80°C. Using the Scherer Equation (2), the average crystallite size (D) of the $BiFeO_3$ powder was calculated from the XRD pattern

$$D = \frac{K\lambda}{\beta} cos\theta \quad (2)$$

Where λ is the X-ray wavelength (1.5406Å), β is the full width at half maximum (FWHM), $K$is Scherer constant and θ is the Bragg angle. The morphology and particle size was studied by scanning electron microscope (SEM).

3.4. Preparation of Phenol Stock Solution

The stock solution was made by dissolving 1g of analytical grade 4-BP in distilled water and raising it up to the mark in a 1L volumetric flask (1000 mg/L). It was kept in a brown glass container to avoid photo-oxidation and was replaced with a fresh one weekly [3]. By dilutions, synthetic adsorbate solutions of varied concentrations were made from the stock solution.

3.5. Design of Experiments using Split Plot Central Composite Design

In this work, split-plot central composite designs (CCD) was used in the Design Expert version 12 computer software, which is a subset of RSM [41]. The Split-plot CCD consist of factorial (f), whole-plot axial (α), subplot axial (β), and center (c) points [17]. The experiment was designed as a three-factor central composite with a split-plot structure and carried out as such. During the design process, three factors were considered: pH, contact time, and adsorbent dosage. There were five levels for each of the numeric factors: plus and minus alpha (axial points), plus and minus 1 (factorial points), and the centre point.

The experimental runs were separated into groups based on pH (the HTC factor), with all runs in one group running at the same time at the same pH level. The 8 factorial runs, 4 whole-plot axial runs, 4 subplot axial runs (set a distance away from the center and allowing the design to spin), and 9 center runs (used to determine the data reproducibility) define the split plot CCD used. There are a total of eight groups of the HTC factor. In all, 25 experiments (runs) were generated from the software for the three variables. The low, central, and high levels, designated as -1, 0 and +1, respectively, were defined in Table 1. Furthermore, in order to predict response functions outside the cubic domain, this approach necessitates experiments outside the experimental range (denoted as ± α). The ranges of these values are shown in Table 1.

3.6. Adsorption Studies

The adsorption experiment was conducted using a method similar to that employed by [19, 25, 42]. To avoid photooxidation, batch adsorption studies were carried out at room temperature with an initial adsorbate concentration of 40 mg/L in the absence of illumination (UV light). The split-plot central composite design matrix in table 2 was used to adjust the pH, adsorbent dosage and contact time. All of the tests were carried out at room temperature using 100 mL of 40 mg/L adsorbate solution in a 250 mL Erlenmeyer flask, with the adsorbent dosage, pH, and contact time set according to the values generated in the experimental design. A laboratory shaker was used to agitate the solution-adsorbent mixtures at 250 rpm. Using a pH meter, the pH of the solution was adjusted with HCl and NaOH solutions. The samples were filtered through Whatman No. 1 filter paper at the conclusion of each shake to remove any fine particles. Blank measurements were taken in all of the tests. Using a double beam UV–Visible spectrophotometer (Agilent technologies, USA) with a wavelength of 225 nm, the equilibrium concentration of 4-BP was determined. Equation 3 was used to determine the adsorbate removal percentage

$$\text{Removal \%} = \frac{C_o - C_e}{C_o} \times 100 \quad (3)$$

Where: Co and Ce are the initial and final concentrations of the adsorbate (mg/L) in the solution.

Equation 4 was used to calculate the adsorption capacity

$$q_e = \frac{Co - Ce}{w} \times v \quad (4)$$

Where: q_e is the adsorption capacity (mg/g), Co is the initial adsorbate concentration of solution (mg/L), Ce is the equilibrium adsorbate concentration (mg/L), v is the volume of adsorbate solution used (L) and w is the weight of the adsorbent (g).

3.7. Adsorption Isotherms

Because they show how much of the adsorbate that is absorbed by the adsorbent at a particular temperature, adsorption isotherm models are often used to characterize adsorption processes. There are several known isotherms based on varied assumptions and conditions, therefore adsorption data is fitted to models with assumptions that are close to the real situation. To allow for the comparison of various materials [43, 44]

3.7.1. Langmuir Adsorption Isotherm

The Langmuir isotherm presupposes that there are an infinite number of binding sites with the same affinity for monolayer adsorption and that the adsorbed molecules do not interact. The Langmuir isotherm is given in linearized form by Equation 5 based on the above assumption [45].

$$\frac{1}{q_e} = \frac{1}{q_{max}} + \frac{1}{k_l q_{max}} \frac{1}{C_e} \quad (5)$$

Where: C_e is the equilibrium concentration (mg/L), q_e is the amount adsorbed at equilibrium time mg/g q_{max} and K_L are Langmuir constants which relate adsorption capacity and the energy of adsorption respectively. q_{max} and K_L can be obtained from the slope and intercept of the graph $\frac{C_e}{q_e}$ against C_e (Fig 6). R_L, which is an indicative of the isotherm shape and predicts whether an adsorption system is favourable or unfavorable, is an essential element of the Langmuir isotherm. R_L according to [46], can be calculated using Equation 6

$$R_L = \frac{1}{(1 + Ce \times K_L)} \quad (6)$$

Where *Ce* is the initial adsorbate concentration (mg/L) and K_L is adsorption equilibrium constant (L/mg) obtained from the intercept of the Langmuir plot. The value of R_L indicates the type of the isotherm to be either:

i. Unfavourable (chemisorption is the predominant process) if $R_L > 1$

ii. Linear (chemisorption and physisorption taking place at the same rate) if $R_L = 1$
iii. Favourable (physisorption is the predominant process) if $0 < R_L < 1$ or
iv. Irreversible (nonreversible chemisorption process) if $R_L = 0$.

3.7.2. The Freundlich Model

The Freundlich isotherm assumes monolayer sorption with a heterogeneous energy distribution of active sites, as well as intermolecular interaction. Equation 7 is the linear Equation for the model.

$$\log_{10} q_e = \log_{10} K_f + \frac{1}{n}\log_{10} C_e \quad (7)$$

Where: q_e and C_e are similarly defined as that in the Langmuir isotherm. A plot of $\log_{10} q_e$ against $\log_{10} C_e$ gives a straight line graph (Fig 7) for dilute solution. The slope is $\frac{1}{n}$ and the intercept is K_f. K_f and n are Freundlich constants; n indicates how favourable the adsorbent's adsorption capacity is, as well as the capacity of the adsorbent-adsorbate system, which is the magnitude of adsorption capacity, and it decreases with increasing temperature [45]

3.7.3. Temkin Isotherm Model

The Temkin isotherm model assumes that all molecules' adsorption heat reduces linearly as the adsorbent surface is covered more, and that adsorption is characterized by a uniform distribution of binding energies up to a maximum binding energy. To put it another way, the model assumes that the heat of adsorption will not be constant. During the adsorption process, it reduces owing to interaction between the sorbent and the sorbate. Equation 8 describes the Temkin isotherm

$$q_e = {}^{RT}/_{b_T} lnK_T + {}^{RT}/_{b_t} lnC_e \quad (8)$$

Where K_T is the equilibrium binding constant (L/mol) corresponding to the maximum binding energy, b_t is related to the adsorption heat, R is the universal gas constant (8.314 J K^{-1} mol^{-1}) and T is the temperature (K). Plotting q_e versus lnC_e, from Equation 8 results in a straight line (Fig 8) of slope ${}^{RT}/_{b_T}$ and intercept ${}^{RT}/_{b_T} lnK_T$

3.7.4. Kinetics Studies

Kinetics studies are important for adsorption studies because they help predict the possible rate-controlling step and mechanism of adsorption reactions. The adsorption uptake was evaluated with respect to time at constant concentration. Pseudo-first-order and pseudo-second-order models were used to find out how the adsorption process works. The pseudo-first-order model is expressed by the Lagergren equation (as reported by [38]) which states that the rate of adsorption site occupation is proportional to the number of unoccupied sites and is given by Equation 9

$$\ln(q_e - q_t) = \ln q_e - K_1 t \quad (9)$$

Where q_e and q_t are the amount of 4-BP adsorbed (mg/g) by $BiFeO_3$ at equilibrium and at any time t, respectively, K_1 (min^{-1}) is the rate constant of pseudo-first-order model, and t is the time (min). A plot of $\ln(q_e - q_t)$ versus t (Fig 9) is used to estimate the values of K_1 and q_e from the slope and the intercept, respectively.

The pseudo-second-order kinetic model can be expressed in the linear form by Equation 10.

$${}^{t}/_{q_t} = {}^{1}/_{K_2 q_e^2} + {}^{1}/_{q_e} \quad (10)$$

Where K_2 is the equilibrium rate constant of pseudo-second-order model (g/mg min^{-1}). The values of q_e and K_2 were determined from the slope and intercept of the plot of (t/q_t) versus t (Fig 10) respectively

4.Conclusion

For the removal of 4-BP onto $BiFeO_3$, three adsorption parameters (pH, adsorbent dosage, and contact time) were optimized using split plot CCD, with the percentage removal ($Y_{4\text{-BP}}$) as the analytical response. The individual and combined effects of the parameters were significant in the removal of the 4-BP adsorbate, per the data analysis. pH 7.0, time 167.0 min and 0.6 g adsorbent dosage were shown to be the optimum adsorption conditions for removing 4-BP from synthetic wastewater by the adsorbent. Up to 87.86 percent of 4-BP was removed by $BiFeO_3$. As a result, the synthesized $BiFeO_3$, being environmentally friendly and having its precursors readily available could be explore further as a feasible alternative to the commercial activated carbon for 4-BP removal in wastewaters.

Acknowledgment

Stephen Godwill will like to thank His Honour, Magistrate Christopher Stephen and Mr. Etsanu Umar Jirah (Taraba state university) for their financial support in the course of carrying out this research.

References

[1] D. Ruifang, C. Dongyun, L. Najun, X. Qingfeng, L. Hua, H. Jinghui and L. Jianmei, Removal of phenol from aqueous solution using acid-modified Pseudomonas putida-sepiolite/ZIF-8 bio-nanocomposites. *Chemosphere.,* 239 (2020) 124708

[2] S.A. Siadati, M.S. Amini-Fazl, & E. Babanezhad, The possibility of sensing and inactivating the hazardous air pollutant species via adsorption and their [2+ 3] cycloaddition reactions with C20 fullerene. Sensors and Actuators B: Chemical, 237 (2016) 591-596

[3] W. Medjor, C. Wepuaka, and G. Stephen, Spectrophotometric Determination of Phenol in Natural Waters by Trichloromethane Extraction Method after Steam Distillation. *International Research Journal of Pure and Applied Chemistry*., 7 (2015). 150-156

[4] K.S. Naresh, Kinetics of simultaneous degradation of 4-bromophenol and 4-chlorophenol by *Arthrobacter chlorophenolicusA6.Biointerface Research in Applied Chemistry* 10 (2020) 4939 – 4943

[5] A. Leri, S. Myneni, The chemistry of bromine in terrestrial and marine environments. *Science Highlight*. 1 (2012) 1-3.

[6] J. Xiong, T. An, C. Zhang, Pollution profiles and risk assessment of PBDEs and phenolic brominated flame retardants in water environments within a typical electronic waste dismantling region. *Environ Geochem Health*. 37 (2015) 457-473.

[7] J. Xiong, G. Li, T. An, The microbial degradation of 2,4,6-tribromophenol (TBP) in water/sediments interface: Investigating bioaugmentation using Bacillus sp. GZT. *Science of Total Environment*. 575 (2017) 573-580.

[8] L. Sabrina, V.I. Andrei, P. Luana, PINTO Luiz and T.R. Cadaval, Preparation of activated carbon from black wattle bark waste and its application for phenol adsorption. *Journal of Environmental Chemical Engineering*., 7 (2019) 103396.

[9] O. Abdelwahab and N.K. Amin, Adsorption of phenol from aqueous solutions by Luffa cylindrica fibers: Kinetics, isotherm and thermodynamic studies. *The Egyptian Journal of Aquatic Research.*, 39 (2013) 215-223

[10] H. Muhammad, Y. Haojie, W. li, S.U. Raja, H. Fazal and T. Lisong, Synthesis and characterization of carboxymethyl starch-g-polyacrylic acids and their properties as adsorbents for ammonia and phenol. *International Journal of Biological Macromolecules*., 138 (2019) 349-358

[11] H.D.S.S. Karunarathne and P. Amarasinghe, Fixed bed adsorption column studies for the removal of aqueous phenol from activated carbon prepared from sugarcane bagasse. *Energy Procedia.*, 34 (2013) 83 – 90

[12] K. Sunil, T. Ravi, P. Suhas, S. Mukesh, Adsorption of Phenol from Wastewater in Fluidized Bed Using Coconut Shell Activated Carbon. *Procedia Engineering*., 51 (2013) 300–307.

[13] L. Zhao, D. Xiao, Y. Liu, H. Xu, H. Nan, D. Li, Y. Kan, X. Cao, Biochar as simultaneous shelter, adsorbent, pH buffer, and substrate of Pseudomonas citronellolis to promote biodegradation of high concentrations of phenol in wastewater. *Water Research*. 2020

[14] S.H. Lin and R.S. Juang, Adsorption of phenol and its derivatives from water using synthetic resins and low-cost natural adsorbents: A review, *J. Environ. Manage*., 90 (2009) 1336–1349

[15] A. Bhatnagar, W. Hogland, M. Marques and M. Sillanpää, An overview of the modification methods of activated carbon for its water treatment applications, *Chem. Eng. J.* 219 (2013) 499–511.

[16] Z. Garba, W. Zhou M. Zhang and Z. Yuan, (2019). A review on the preparation, characterization and potential application of perovskites as adsorbents for wastewater treatment. *Chemosphere.,* 244 (2019) 125474.

[17] R.H. Myers, D.C. Montgomery, and C. Anderson-Cook, Response Surface Methodology: Process and Product Optimization Using Designed Experiments. John Wiley and Sons: New York (2016)

[18] Y. Yakubu and A.U. Chukwu, Split-Plot Central Composite Designs Robust to a Pair of Missing Observations. *J. Appl. Sci. Environ. Manage*. 22 (2018) 1409–1415

[19] V. Arun, N. Saharan, V. Ramasubramanian, B. Rani, K.R. Salin R. Sontakke, H. Haridas and D. Pazhayamadom, Multi-response optimization of Artemia hatching process using split-split-plot design based response surface methodology. *Scientific Reports.* 7 (2017) 40394.

[20] Omid, *et al.* (2015) Synthesis and Characterization of BiFeO3 Ceramic by Simple and Novel Methods. *De Gruyter* 35 (2015): 551–557.

[21] H. Yongming, L. Fei, Z. Yiling, Y. Jikang, W.Y. Wang and G. Haoshuang, Synthesis of Bismuth Ferrite Nanoparticles via a Wet Chemical Route at Low Temperature. *Journal of Nanomaterials.* (2011) 1-6

[22] K. Dovydas, G. Diana, M. Kestutis, B. Dalis, D.V. Karpinsky, L. Anna, P. Głuchowski, R. Rimantas, K. Arturas, Z. Aleksej and K. Aivaras, A Facile Synthesis and Characterization of Highly Crystalline Submicro-Sized BiFeO3. *Materials*. 13 (2020) 3035

[23] S. Pattnaik, B. Arjun, S. Martha, R. Acharya and K. Parida, Synthesis, photoelectrochemical properties and solar light-induced photocatalytic activity of bismuth ferrite nanoparticles. *Journal of Nanoparticle Research* 20 (2018)

[24] J. Penalva, and A. Lazo, Synthesis of Bismuth Ferrite $BiFeO_3$ by solution combustion method. *Journal of Physics: Conference Series (J. Phys.) Conf. Ser.* 1143 (2018) 012025

[25] F.G. Okibe, Z.N. Garba and J.M. Alimi, Optimization of the Conditions for Adsorption of Fluoride in Aqueous Solution by Carrot Residue Using Central Composite Design of Experiment. *Bayero Journal of Pure and Applied Sciences*., 11 (2018) 230 – 237

[26] O. Amiri, M. Mozdianfar, M. Vahid, M. Salavati-Niasari and S. Gholamrezaei, Synthesis and Characterization of BiFeO*3* Ceramic by Simple and Novel Methods: *High Temperature Materials and Processes*, 35 (2015), 551-557

[27] Y. Yakubu, Z.Q. Aliyu, A. Usman and P.O. Evans, Split-plot Central Composite Experimental Design Method for Optimization of Cake Height to Achieve desired Texture. *Nigerian. Journal of Basic and Applied Science*. 28 (2020): 30-39

[28] Z.N. Garba, W. Zhou, I. Lawan, W. Xiao, M. Zhang, L. Wang, L. Chen, Z. Yuan, An overview of chlorophenol as contaminants and their removal from wastewater by adsorption: A review. *Journal of environmental management* 241 (2019) 59-75

[29] A.A. Salem, A. Hamidi and B. Mohammed, Application of Response Surface Methodology (RSM) for Optimization of Semi-Aerobic Landfill Leachate Treatment Using Ozone. *Applied water sciences*. (2014) doi: 10.1007/s13201-014-0156

[30] B. Buhani, P. Megafhit, R. Rahmawaty, S. Suharso, R. Mita and S. Sumadi, Adsorption of phenol and methylene blue in solution by oil palm shell activated carbon prepared by chemical activation. *Oriental journal of chemistry*. 34(2018) 2043-2050

[31] Bingxin, *et al.* Adsorption of Phenol on Commercial Activated Carbons: Modelling and Interpretation. *Int J Environ Res Public Health*. 17 (2020): 789.

[32] S.K. Nadavala and M. Kim, Removal of phenolic compounds from aqueous solutions by biosorption onto acacia leucocephala bark powder: Equilibrium and kinetic studies. *Journal of the Chilean Chemical Society*., 56 (2011) 539-545

[33] X. Wang (2018) Removal of Bromophenols from Wastewater bySorption: [Master's thesis], University of Waterloo, Ontario, Canada

[34] M. Abdelkreem, Adsorption of Phenol from Industrial Wastewater Using Olive Mill Waste. *APCBEE Procedia*., 5 (2013) 349–357

[35] T. Mitiku and S. Khalid, Adsorption of Phenol Using 8-Hydroxyquinoline Treated and Untreated Tea Waste. *Int J Environ Sci Nat Res.* 17 (2019) 555974.

[36] B. Salim and H.M. Abdeslam, Removal of Phenol from Water by Adsorption onto Sewage Sludge Based Adsorbent *Cemical Engineering Transactions* 40 (2014). Available online in: https://doi: 10.3303/CET1440040

[37] G. Stephen (2022) Preparation, characterization and evaluation of $BiFeO_3$ perovskite material for the optimal removal of phenolic compounds from synthetic wastewater using split plot central composite design: [Master's thesis], Ahmadu Bello University, Zaria, Nigeria

[38] E. Nyankson, A. Jonas, E. Johnson, Y. Abu, M. Gloria, A. Kingsford and Y.A. Richard, Synthesis and Kinetic Adsorption Characteristics of Zeolite/CeO2 Nanocomposite. *Scientific African.* 7 (2020) 257

[39] J. Wang H. Guo, Y. Liu, W. Li and B. Yang, Peroxymonosulfate activation by porous BiFeO3 for the degradation of bisphenol AF: Non-radical and radical mechanism. Applied Surface Science. 507 (2019) 145097.

[40] S. Dwita and Ismojo, FTIR Spectrum of BiFeO3 Ceramic Produced By Sol-Gel Method Based On Variation of Sinter and Calcination Treatment. *The International Journal Of Engineering And Scienc.*, 5 (2016) 114

[41] Z.N. Garba and A.A. Rahim, process optimization of $K_2C_2O_4$ activated carbon from *Prosopis africana* seed hulls using response surface methodology. *Journal of Analytical andapplied pyrolysis* 107(2014) 306-312

[42] T.A. Nour, A.C. Ghadir and S.H. Farag, Individual and competitive adsorption of phenol and nickel onto multiwalled carbon nanotubes *Egyptian Journal of Aquatic Research* 6 (2015) 405-415

[43] K.Y. Foo, and B.H. Hameed, "Insights into the modeling of adsorption isotherm systems". *Chemical Engineering Journal.*, 156 (2010) 2–10

[44] A. Awad, R. Jalab, A. Benamor, M. Naser, M. Ba-Abbad, M. El-Naas and A. Mohammad, Adsorption of organic pollutants by nanomaterial-based adsorbents: An overview. Journal of Molecular Liquids. 301 (2020) 112335

[45] E.A. Idowu, Adsorption of Selected Heavy Metals on Activated Carbon Prepared from Plantain (*Musa paradisiacaL*.) Peel. (2015). Chemistry department, Ahmadu Bello University Zaria, Kaduna State, Nigeria.

[46] G. Upenyu, P. Lycenter and C. Fidelis., Application of Central Composite Design in the Adsorption of Ca(II) on Metakaolin Zeolite. *Journal of Chemistry* (2017) 1-10